RSC Advances

ROYAL SOCIETY OF CHEMISTRY

www.rsc.org/advances

Cite this: DOI: 10.1039/c0xx00000x

www.rsc.org/xxxxxx

ARTICLE TYPE

Improved Hydrogen Production from Formic Acid under Ambient Condition Using PdAu Catalyst on Graphene Nanosheets-Carbon Black Support †

Yu-ling Qin,[a, c] Jian-wei Wang,[a, c] Yao-ming Wu,[a, b] Li-min Wang*[, a, b]

Received (in XXX, XXX) XthXXXXXXXXX 20XX, Accepted Xth XXXXXXXXX 20XX
DOI: 10.1039/b000000x

Formic acid (FA) has great potential as a suitable liquid source for hydrogen and hydrogen storage material, provided highly active and selective dehydrogenation catalysts under ambient conditions are developed. Here, well-dispersed bimetallic gold-palladium (PdAu) nanoparticles (NPs) grown on graphene nanosheets-carbon black (GNs-CB) composite supports are synthesized via a facile co-reduction method, wherein the GNs-CB composite support proved to be a powerful dispersion agent and distinct support for the PdAu NPs. Interestingly, the resultant PdAu/GNs-CB catalyst manifests highly selectivity and exceedingly high activity to complete the decomposition of FA at room temperature.

Introduction

Hydrogen is generally proposed to be an important energy vector to face the increasing level of energy crisis and environmental pollution due to its high energy density and efficiency with low environmental load.[1] However, even after several decades of intensive exploration, hydrogen storage is still one of the most challenging barriers that impede the implementation of the hydrogen-based economy. FA, as a major product of biomass processing, has attracted considerable attention as a suitable liquid source for hydrogen and as a potential hydrogen storage material due to their intrinsic advantages, including high energy density, nontoxic, and easy recharging as a liquid (the availability of the existing infrastructure for gasoline and oil).[2]

Over the past decades, homogeneous catalysts for FA decomposition have been intensively investigated and significant advances have been achieved.[3] However, those homogeneous catalysts suffer more or less severe drawbacks such as easy deactivation, hard to separate and recycle, use of organic solvents, etc.[4] To solve these problems, increasing interests have recently been devoted to heterogeneous catalyst.

Pd NPs have been reported to exhibit excellent catalytic activity toward FA decomposition. However, monometallic Pd is prone to be deactivated because of the adsorption of poisoning carbon monoxide intermediates.[5] In many works, Au is employed to improve the performance of Pd nanocatalysts, which various supports are used to load NPs.[5, 6] For example, at elevated temperature (90 °C), PdAu NPs loaded on ED-MIL-101[5a] or C-CeO_2 support,[5c] and PdAu@Pd/C[5d] have been reported to exhibit enhanced catalytic activity. The initial reaction rates of 106[5a], 113.5[5c] and 82.6[5d] mol_{H_2} $mol_{catalyst}^{-1}$ h^{-1} have been achieved. To date, highly selective and efficient PdAu catalysts which can be used to significantly improve kinetic properties for catalytic decomposition of FA under ambient temperature are necessary.

Aside from tuning the catalyst composition, adjusting and optimizing the interaction between the active metal phase and the support materials are key approaches to further improve catalytic performance.[7] An ideally high performance support guarantees good dispersion of active catalyst particles, facile electron transfer, and favorable mass transport kinetics. The strategy of coupling CB and GNs to form a novel carbon-based composite support for NPs has been reported in our previous work.[4c] Here, we use GNs-CB as a super support to load PdAu NPs, and graphene oxide (GO) is employed as the precursor of GNs. The resultant PdAu/GNs-CB catalyst exhibits improved catalytic performance toward complete decomposition of FA at room temperature. The prepared PdAu/GNs-CB nanocatalysts are also used to study the role that sodium formate plays in FA decomposition reaction.

Experimental Section

Graphene Oxide (GO) preparation

GO was made by a modified Hummers method. Briefly, graphite powder (3 g, 325 mesh) was put into an 80 °C solution of concentrated H_2SO_4 (12 mL), $K_2S_2O_8$ (2.5 g), and P_2O_5 (2.5 g). After keeping at 80 °C for 4.5 h using a hot plate, the mixture was cooled to room temperature and diluted with 0.5 L of de-ionized water and left overnight. Then, the mixture was filtered and washed with de-ionized water using a 0.2 micron Nylon Millipore filter to remove the residual acid. The product was dried under room condition overnight. Next, the pretreated graphite powder was put into cold (0 °C) concentrated H_2SO_4 (120 mL) in a 250mL round-bottom flask equipped with a magnetic stir bar. 15 g $KMnO_4$ was added gradually under stirring while the temperature of the mixture was kept below 20 °C. The solution was then stirred at 35 °C for 2 h. Afterwards, 250 mL of de-

ionized water was added and the suspension was stirred for another 2 h. Subsequently, additional 0.7 L of de-ionized water was added. Shortly after that, 20 mL of 30% H_2O_2 was added to the mixture to destroy the excess of permanganate. The suspension was then repeatedly centrifuged and washed first with 5% HCl solution and then with water. Exfoliation of graphite oxide to GO was achieved by ultrasonication of the dispersion for 120 min.

Catalyst preparation

For the first step, 150 mg of Vulcan XC-72 carbon powder was ultrasonically dispersed in 20 mL of water and subsequently mixed with 15 mL GO solution (2 mg mL^{-1}), then the mixture was stirred/sonicated for 6 h. H_2PdCl_4 (0.05285 M) and specific atom proportion of gold element ($KAuCl_4$, 0.0273 M) aqueous solution were added into the mixture, followed by adding 10 mL of $NaBH_4$ (10 $mgmL^{-1}$) solution after 1 h. The mixture was stirred for another 8 h at room temperature in order to deposit the NPs onto the support absolutely. Finally, the desired catalyst from the suspension was centrifuged and washed with the distilled water and then dried in vacuum at 80 ^oC overnight. The synthesises of PdAu/CB and PdAu/GNs were similar with that of PdAu/GNs-CB. PdAu/GNs was obtained by frieze drying. In this work, the ratio of CB/GO support in PdAu/GNs-CB or Pd(Au)/GNs-CB is 5/1, except the samples in the Fig. 6.

Instrumentation

Transmission electron microscope (TEM) was performed using a FEI Tecnai G2 S-Twin instrument with a field emission gun operating at 200 kV. Mass analysis of the generated gases was performed using a ThermoStar^{TM} gas analysis system GSD 320 mass spectrometer (Detection limit minimum: Faraday < 20 ppm, C-SEM < 1 ppm, 1-100 amu), wherein argon gas is chosen as cleaning gas. Gas analysis of the generated gases was performed using a Techcomp GC 7900 gas chromatography Analyzer, wherein argon gas is chosen as carrying gas. The detection limit for CO was below 10 ppm.XPS spectra were obtained with an ESCALABMKLL X-ray photoelectron spectrometer using an Al Kα source. The liquid chromatogram was obtained by Shimadzu LC-20AB with RI detector (Shimadzu RID-10A), and Aminex HPX-87H column (Bio-Rad, 300×7.8 mm), using 0.5 mM H_2SO_4 as fluent at a flow rate of 0.7 $mlmin^{-1}$ at 323 K. Powder X-ray diffraction (XRD) patterns were collected on Bruker D8 Focus Powder X-ray diffractometer using Cu Kαradiation (40 kV, 40 mA). The electrochemical tests were carried out with a BioLogic VMP3 electrochemical workstation. Inductively coupled plasma atomic emission spectroscopy (ICP-AES) measurements were performed on a TJA (Thermo Jarrell Ash) Atomscan Advantage instrument.

Electrochemical Characterizations for the Catalysts

For preparation of the thin-film working electrode, the GC electrode was sequentially polished with 3 and 0.5 μm Al_2O_3 paste (mixed with Al_2O_3 powder and ultrapure water). After the mechanical pretreatment, the electrode was cleaned by sonication in ultrapure water. To prepare the working electrode, 5 mg of the catalysts was dispersed in diluted Nafion alcohol solution which contained 1000 μL of ethanol and 25 μL of nafion, and was sonicated for 1 h to obtain a uniform suspension. Next, 8 μL of the suspension was pipetted onto the flat glassy carbon electrode. The coated electrode was then dried at room temperature for 10 min. Electrochemical experiments were carried out in a standard three-electrode cell at room temperature. The working electrode was the thin-film electrode with catalysts. Pt foil and Ag/AgCl electrode were used as the counter and reference electrodes, respectively. All potentials in this report referred to Ag/AgCl. All electrolyte solutions were deaerated with high-purity nitrogen for at least 30 min prior to any measurement.

FA decomposition reaction

Catalytic reactions were carried out at room temperature using a two-necked round bottom flask with one of the flask openings connected to a gas burette and the other for the introduction of FA (Figure S1). Catalytic decomposition reaction of FA for the release of hydrogen (along with carbon dioxide) was initiated by stirring the mixture of FA solution introduced via a pressure-equalization funnel and the aqueous suspension of the catalyst prepared as described above. The volume of reforming gas was monitored by using the gas burette.

Results and Discussion

Structural characterizations of the PdAu catalyst

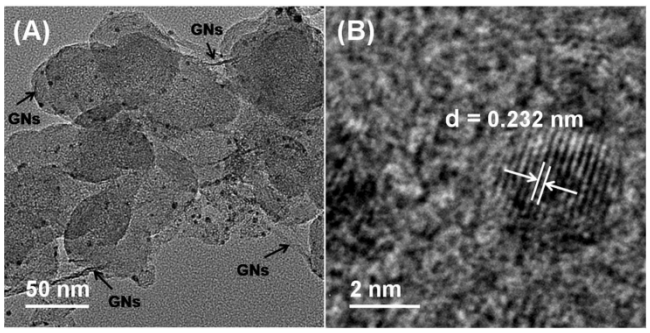

Figure 1. (A) TEM and (B) HRTEM images of PdAu/GNs-CB.

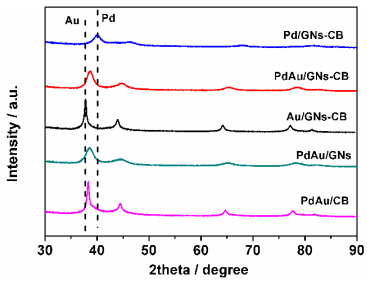

Figure 2. XRD patterns for PdAu, Pd and Au NPs loaded on different supports.

As shown in Figure S2, in contrast to pristine CB (XC-72), the GO-CB composite support shows better dispersion in water and facilitates the subsequent synthesis of highly dispersed PdAu catalyst. The N_2 adsorption-desorption isotherms of GO-CB is shown in Figure S3, and the specific surface area is measured to

be 324 m^2/g. From Table 1, we can find that the specific surface areas for CB and GNS are smaller than the composite support. Specially, for GNs (GO reduced by $NaBH_4$), the specific surface area reduces terriblly because of the aggregation.The difference of BET among the three supports may affect the average size and dispersion of the NPs.

Table 1.ICP analyses and average size of NPs and BET surface areas for the samples.

Sample	Metal content (%)	Average size of NPs (nm)	BET for support (m^2 g^{-1})
PdAu/CB	Au, 4.04; Pd, 0.87	3.89±0.7	202
PdAu/GNs-CB	Au, 4.34; Pd, 0.92	2.79±0.7	304
PdAu/GNs	Au, 5.98; Pd, 1.25	4.03±0.8	37.8

Figure 1A shows the transmission electron microscopy (TEM) image of the as-synthesized PdAu/GNs-CB catalysts. CB and GNs can be differentiated obviously from Figure 1A (CB is spherical; GNS is sheet like with wrinkle.). Clearly, GNs and CB are closely associated. As expected, well-dispersed PdAu NPs on GNs-CB were obtained. In the case of GO or CB alone under similar synthesis conditions, only larger PdAu NPs can be found (Table 1, average size of NPS are obtained from TEM micrographs (Figure 1A and S4)), highlighting the advantages in combining GNs and CB. The high-resolution TEM (HRTEM) image from Figure 1B shows that the (111) d-spacing of Pd-Au nanoparticle is smaller than that of pure fcc-Au, but bigger than that of pure fcc-Pd. As shown in Figure 2, X-ray diffraction (XRD) patterns of Au and Pd supported on GNs-CB both are in good agreement with the face-centered cubic metallic Au (PDF#65-2870) and Pd (PDF#46-1043), respectively. Because Au scatters X-rays more effectively than Pd, the diffractive peaks of Pd in PdAu NPs are hard to be detected. Furthermore, XRD patterns of bimetallic NPs reveal that all diffraction peaks are situated between those of Au and Pd, and thus, are reasonably indexed to PdAu alloy. The inductively coupled plasma atomic emission spectroscopy (ICP-AES) results show that the Au/Pd ratio of catalysts prepared with different support are 2.49, 2.54 and 2.57, respectively, which are almost in agreement with the ratio of metal precursors.

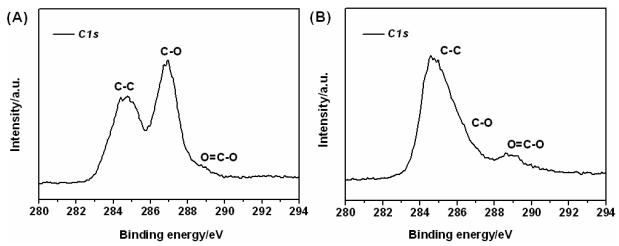

Figure 3. XPS spectra of C_{1s} on A) GO and B) GO reduced by $NaBH_4$.

During the reduction process of Pd and Au precursors, GO could also be reduced by $NaBH_4$. As shown in Figure 3, C-C bonds (284.5 eV) become predominant while the peak of C-O is significantly reduced. However, it is worth noting that some residual oxygen-containing groups can still be found on the reduced GO, which could improve wettability and accessibility of aqueous FA solution to the active surface and improve the performance of the catalyst.[8] In addition, Sharma[8b] also proved by experimental observations that the presence of residual oxygen groups on reduced GO plays an important role on the removal of carbonaceous species from the adjacent sites, which may be benefit for FA decomposition**.**

PdAu-Catalyzed FA decomposition to generate hydrogen

Figure 4A shows the plots of volume of generated gas (CO_2+H_2) versus the reaction time during dehydrogenation of aqueous FA solution catalyzed by PdAu NPs loaded on different supports. The illustration of apparatus for catalytic reaction is shown in Figure S1. FA decomposition or evaporation at room temperature without catalyst is not evident in Figure 4A (trace d). From Figure S5, we can find that the prepared PdAu NPs without support show the poor catalytic activity toward FA decomposition at room temperature. Interestingly, the PdAu catalyst prepared in the presence of GO-CB composite support (a) exhibits enhanced activity in completing the decomposition of FA within only 30 min at room temperature in aqueous media (trace a and inset, Figure 4A). Gas chromatograms (Figure S6) and mass spectral profiles (Figure S7) show that no detectable amount of CO (< 10 ppm) is found in the gas mixture generated from the dehydrogenation of FA. Completion of the reaction is confirmed by the amount of released gas [$n(H_2+CO_2)/n$HCOOH = 2.0] and the liquid chromatogram spectra (Figure 4B, $S_{before} \geq 2S_{after}$). The FA dehydrogenation performance at room temperature on PdAu/GNs-CB is much higher than the reported PdAu/ED-MIL-101 (reaction at 90°C),[5a] PdAu/C-CeO_2 (reaction at 90 °C),[5c] PdAu@Pd/C (reaction at 90°C),[5d] and PdAu alloy NPs (reaction at 50 °C)[5e] catalysts. On the contrary, for the PdAu NPs synthesized with CB or GNs alone, only ~80% (trace b, Figure 4A) and ~55% (trace c, Figure 4A) of H_2 are released from FA even after more than 5 h, which is much worse than that of PdAu catalyst prepared with GNs-CB. The values of the initial reaction rates (30 min) on PdAu/C and PdAu/GNs is 79.1 and 58.5 mol_{H_2} $mol_{catalyst}^{-1}$ h^{-1}, which is much smaller than that on PdAu/GNs (175 mol_{H_2} $mol_{catalyst}^{-1}$ h^{-1}).

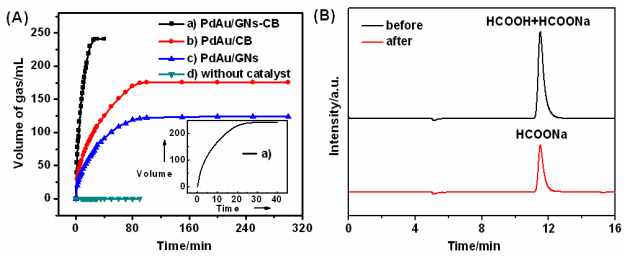

Figure 4. (A) FA decomposition from 5 mL of solution containing 1 M FA and 1 M sodium formate using 10 mg (0.058 mmol) of PdAu loaded on three kinds of supports at room temperature. Inset: the expanded view of a. (B) Liquid chromatogram of FA solution (1 M FA and 1 M sodium formate) over PdAu/GNs-CB before and after reaction.

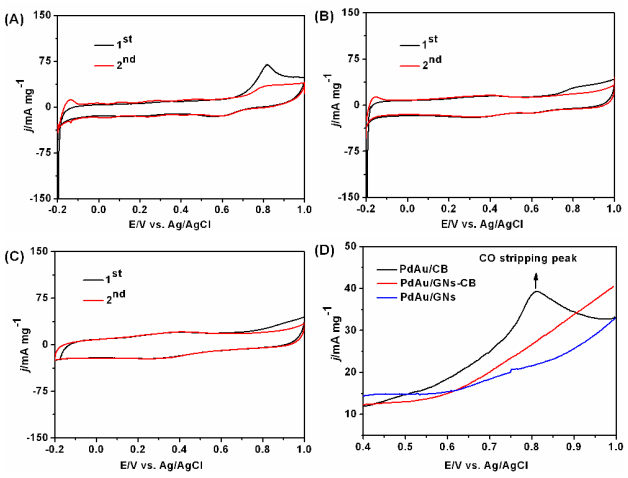

Figure 5. CO stripping voltammograms on three kinds of catalysts in 0.5 M H_2SO_4 solution at a scan rate of 50 mV/s: (A), PdAu/CB; (B), PdAu/GNs-CB; (C), PdAu/GNs. (D) CVs of three kinds of catalysts after reaction in 0.5 M H_2SO_4 solution at a scan rate of 50 mV/s.

Regarding the improved catalytic performance of FA decomposition, we believe that PdAu/GNs-CB should have a much stronger tolerance to CO adsorption. CO stripping voltammetry is an effective method to determine the anti-poisoning ability of a catalyst toward CO. As shown in Figures 5A and B, both the onset potential and the peak area of CO oxidation for PdAu/GNs-CB are much lower than those of the PdAu/CB catalyst, indicating that PdAu/GNs-CB catalyst possesses a strong anti-poisoning capability of CO.[5d] No visible CO oxidation peak for PdAu/GNs (Figure 5C) is observed, revealing scarce CO absorption on the surface. Furthermore, cyclic voltammograms (CVs) (Figure 5D) on the catalysts after reaction are employed. Clearly, a CO stripping peak can be found from the CV on PdAu/CB, which could be explained by the fact that CO from FA decomposition cannot be desorbed from the surface of the catalyst and thus reducing the activity. As for PdAu/GNs, although no CO absorbs on the surface of the catalyst, aggregation of GNs (Figure S8) decreases the catalytic activity.

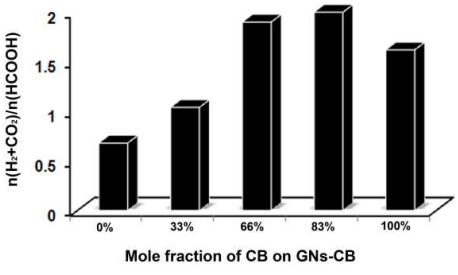

Figure 6. Plot of completeness of FA decomposition over PdAu at different support ratios CB:GNs at 30 min.

The above mentioned results indicate that the enhanced activity of PdAu NPs supported on GNs-CB can reasonably be attributed to the combined effect of good dispersion and small particle size of PdAu NPs, as well as the anti-poisoning ability of the catalyst. However, since support plays an important role in catalytic performance, PdAu loaded on supports with different ratios of CB/GNs are also prepared. Their catalytic activities are shown in Figure 6. Under the same PdAu loading condition, the best catalytic activity could be obtained when the ratio of CB to GNs is 5. Considering the above mentioned results, the poor activity of PdAu loaded on GNs-CB with other CB/GNs ratios may be related to the weak dispersion and/or anti-poisoning ability.

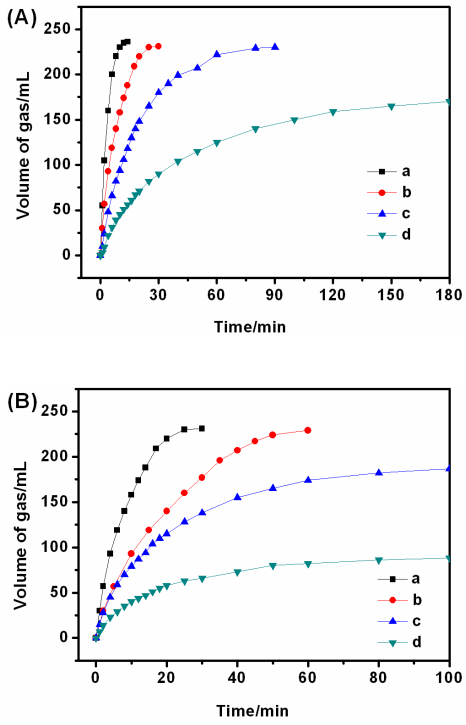

Figure 7. (A) FA decomposition from 5 mL of solution containing 1 M FA and different concentration of sodium formate (a, 3 M; b, 1 M; c, 0.5 M; d, 0.2 M) using 10 mg of PdAu/GNs-CB catalyst. (B) FA decomposition from 5 mL of solution containing 1 M FA and 1 M sodium formate with different concentration of HCl (a, 0 M; b, 0.01 M; c, 0.03 M; d, 0.075 M) using 10 mg of PdAu/GNs-CB catalyst.

Bimolecular HCOOH/$HCOO^-$ mechanism on oxide catalysts model has been discussed by Borowiak.[9] However, Zhou[5c] suggests that the mixture containing HCOOH and $HCOO^-$ keeps the NPs in a reduced state, consequently retaining the stability of the alloy catalyst. In order to elucidate the mechanism HCOONa involved in this dehydrogenation reaction, three additional experiments were performed in our work. No matter what decomposition mechanism the FA follows, C-H cleavage is the rate-determining step in obtaining hydrogen. Therefore, the concentration of formate ion may also be important for FA decomposition. To this end, Figure 7A shows the plots of volume of generated gas (CO_2+H_2) versus the reaction time during FA dehydrogenation at FA solution with different sodium formate concentration. Clearly, the reaction rate increases with increased concentration of formate. In this reaction system, sodium formate has two functions: increasing the pH value and the formate ion

concentration. Hence, investigating the pH value separately is essential.

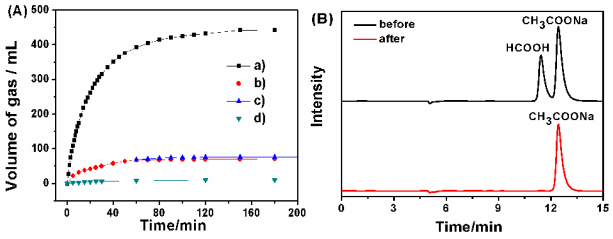

Figure 8. (A) FA decomposition from 5 mL of solution using 20 mg of PdAu/GNs-CB. (a, 2 M FA and 2 M sodium acetate; b, 2 M FA; c, 2 M FA and 2 M sodium acetate (added at the reaction time of 60 min); d, 2 M sodium formate). (B) Liquid chromatogram of FA solution (a) before and after reaction.

Figure 8A shows the plots of volume of generated gas (CO_2+H_2) versus the reaction time during FA dehydrogenation at different FA solution. Sodium acetate is used to replace sodium formate. As shown in Figure 8A, only negligible product gas is observed from the decomposition of sodium formate solution (trace d, Figure 8A). In the case of 2 M FA, only 15% FA is decomposed in pure FA solution during the first 60 min (trace b, Figure 8A, pH = 1.87). No FA further decomposes even if the reaction time is extended to 210 min. For FA/sodium acetate solution (pH = 4.02), FA decomposes completely within 3 h (trace a, Figure 8A) can be confirmed by LC (Figure 8B). It should be noted that although sodium acetate is added into 2 M FA solution after reaction (60 min) to increase the pH, almost no improvement in reaction activity is achieved (trace c, Figure 8A), indicating that degradation of the catalyst in low pH cannot be recovered by subsequently increasing the pH. That is, highly efficient hydrogen production from FA decomposition can be achieved at room temperature with the help of PdAu/GNs–CB, provided that pH is sufficiently high. Again, in order to further confirm this point, FA solution (1 M FA and 1 M sodium fromate) decomposition with different H^+ concentration is shown in Figure 7B. As the input of H^+ is increased, the dehydrogen rate decreases obviously, which confirms that the higher pH value is benefit for the FA decomposition.

Lifetime is very important for the practical application of nanocatalysts. In this sense, recycle test of the PdAu/GNs-CB catalyst has been conducted for the same decomposing reaction. Repeated testing was obtained by adding pure FA (4 mmol) into the reaction vessel after the completion of the previous run. From Figure 9, only a slight deactivation has been observed in the second run, which denotes good stability of PdAu/GNs-CB during the first two runs. Unfortunately, the catalytic activity highly decreases in the third run and forth run (Figure S9). Therefore, further investigations are needed to improve the durability of PdAu/GNs-CB.

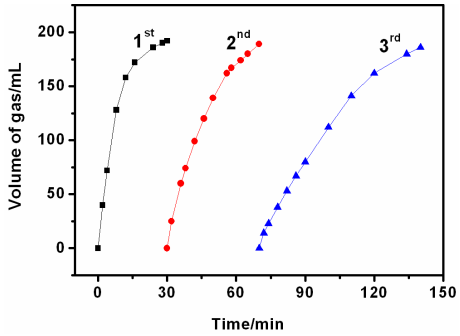

Figure 9. Three repeated testings of GNs-CB supported PdAu (8 mg) in 4 mL of FA solution at room temperature.

Conclusion

In summary, a facile method is used to synthesize well-dispersed PdAu NPs grown on a GNs-CB composite support to combine the advantages of GNs and CB. Unexpectedly, PdAu NPs loaded on GNs-CB exhibit higher catalytic performance for FA decomposition at room temperature in aqueous media than on GNs or CB alone. Furthermore, the as-prepared PdAu NPs also exhibit high hydrogen selectivity in FA decomposition reaction that no detectable amount of CO is found in the gas mixture generated from the dehydrogenation of FA. Sodium formate also has an important function in promoting decomposition. This study proposed composite support and could open an effective method to prepared nanocatalysts for hydrogen generation from renewable fuels suchas FA.

Acknowledgements

This research is financially supported by the National Nature Science Foundation of China (Grant No.20111061).

Notes and references

[a]*State Key Laboratory of Rare Earth Resource Utilization, Changchun Institute of Applied Chemistry, Changchun 130022, Jilin, China. E-mail: lmwang@ciac.jl.cn*
[b]*Changzhou Institute of Energy Storage Materials&Devices, Changzhou 213000, Jiangsu, China*
[c]*University of Chinese Academy of Sciences, Beijing 100049, China*
E-mail: ylqin@ciac.jl.cn

† Electronic Supplementary Information (ESI) available: [Detailed illustration of apparatus, TEM and SEM characterization, GC and MS analyses of gas.]. See DOI: 10.1039/b000000x/

1 a) S. Jones, J. Qu, K. Tedsree, X. O. Gong and S. C. E. Tsang, *Angew. Chem. Int. Ed*., 2012, **51**, 11275; b) Y. He and Y. Zhao, *Phys. Chem. Chem. Phys.*, 2009, **11**, 255; c) Y. Yamada, T. Miyahigashi, K. Ohkubo and S. Fukuzumi, *Phys. Chem. Chem. Phys.*, 2012, **14**, 10564; d) Y. L. Qin, X. B. Zhang, J. Wang and L. M. Wang, *J. Mater. Chem.,* 2012, **22**, 14861; e) L. Dienberg, J. Haug, G. Rauhut and E. Roduner, *Phys. Chem. Chem. Phys.*, 2013, **15**, 5836.
2 a) Q. Y. Bi, X. L. Du, Y. M. Liu, Y. Cao, H. Y. He and K. N. Fan, *J. Am. Chem. Soc.,* 2012, **134**, 8926; b) D. A. Bulushev, L. Jia, S. Beloshapkin and J. R. H. Ross, *Chem. Commun*., 2012, 4184; c) Z. L. Wang, J. M. Yan, H. L. Wang, Y. Ping and Q. Jiang, *Sci. Rep*., 2012, **2**, 598; d) R. Muralidharan, M. Mclntosh and X. Li, *Phys. Chem. Chem. Phys.*, 2013, **15**, 9716; e) H. Jeon, S. Uhm, B. Jeong and J. Lee, *Phys. Chem. Chem. Phys.*, 2011, **13**, 6192.
3 a) B. Loges, A. Boddien, H. Junge and M. Beller, *Angew. Chem. Int. Ed.,* 2008, **47**, 3962; b) C. Fellay, P. J. Dyson and G. Laurenczy,

Angew. Chem. Int. Ed., 2008, **47**, 3966; c) S. Enthaler, J. V. Langermann and T. Schmidt, *Energy Environ. Sci.,*2010, **3**, 1207.
4 a) S. Zhang, Ő. Metin, D. Su and S.Sun, *Angew. Chem. Int. Ed.,* 2013, **52**, 3681; b) Z. L. Wang, J. M. Yan, Y. Ping, H. L. Wang, W.
5 T. Zheng and Q. Jiang, *Angew. Chem. Int. Ed.,* 2013, **52**, 4406; c) Y. L. Qin, J. Wang, F. Z. Meng, L. M. Wang and X. B. Zhang, *Chem. Comm*., 2013, DOI: 10.1039/c3cc46248j.
5 a) X. Gu, Z. H. Lu, H. L. Jiang, T. Akita and Q. Xu, *J. Am. Chem. Soc.,* 2011, **13**, 11822; b) H. L. Jiang, S. K. Singh, J. M. Yan, X. B.
10 Zhang and Q. Xu, *ChemSusChem*., 2010, **3**, 541;c) X. Zhou, Y. Huang, C. Liu, J. Liao, T. Lu and W. Xing, *Chem. Commun.,* 2008, 3540; d) Y. Huang, X. Zhou, M. Yin, C. Liu and W. Xing, *Chem. Mater.,* 2010, **22**, 5122; e) Ő. Metin, X. Sun and S. Sun, *Nanoscale,* 2013, **5**, 910; f) D. A. Bulushev, S. Beloshapkin, P. E. Plyusnin, Y. V.
15 Shubin, V. I. Bukhtiyarov, S. V. Korenev and J. R. H. Ross, *J. Catal.*, 2013, **299**, 171.
6 K. Tedsree, T. Li, S. Jones, C. W. A. Chan, K. M. K. Yu, P. A. Bagot, E. A. Marquis, G. D. W. Smithand S. C. E. Tsang, *Nat. Nanotechnol.,* 2011, **6**, 302.
20 7 a) A. Bruix, J. A. Rodriguez, P. J. Ramírez, S. D. Senanayake, J. Evans, J. B. Park, D. Stacchiola, P. Liu, J. Hrbek and F. Illas, *J. Am. Chem. Soc.,*2012, **134***,* 8968; b) L. He, Y. Huang, A. Wang, X. Wang, X. Chen, J. J. Delgado and T. Zhang, *Angew. Chem. Int. Ed.,*2012, **51**, 6191; c) J. Macht and E. Lglesia, *Phys. Chem. Chem.*
25 *Phys.*, 2008, **10**, 5331; d) A. Primo, A. Corma and H. Garcia, *Phys. Chem. Chem. Phys.*, 2011, **13**, 886.
8 a) M. Pumera, *Chem. Soc. Rev.,* 2010, **39**, 4146; b) S. Sharma, A. Ganguly, P. Papakonstantinou, X. Miao, M. Li, J. L. Hutchison, M. Delichatsios and S. Ukleja, *J. Phys. Chem. C,* 2010, **114**, 19459.
30 9 M. A. Borowiak, M. H. Jamróz and R. Larsson, *J. Mol. Catal. A: Chem.,* 2000, **152**, 121.

Table of contents

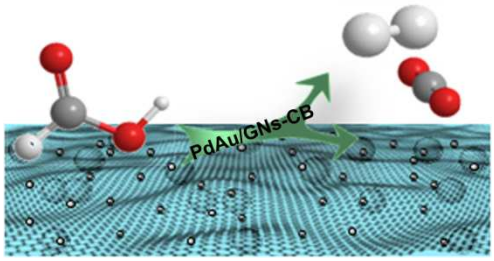

Well-dispersed PdAu nanoparticles grown on graphene
35 nanosheets-carbon black support are synthesized via a facile co-reduction method, wherein the support is a unique and powerful dispersion agent. The as-prepared catalyst manifests high activity in formic acid decomposition at room temperature.